Comparison of Dynamic Differential Evolution and Asynchronous Particle Swarm Optimization for Inverse Scattering of a Two-Dimensional Perfectly Conducting Cylinder

Ching-Lieh Li [1], Chung-Hsin Huang [2], Chien-Ching Chiu [1], and Chi-Hsien Sun [3]

[1] Electrical Engineering Department, Tamkang University,
Tamsui District, New Taipei City, Taiwan, R.O.C.

[2] Department of Computer and Communication Engineering, Taipei College of Maritime Technology,
Tamsui District, New Taipei City, Taiwan, R.O.C.

[3] Department of Electronic Engineering, National Taiwan University of Science and Technology,
Taipei, Taiwan, R.O.C.

Abstract ─ The application of optimization techniques for shape reconstruction of a perfectly conducting two-dimensional cylinder buried in a slab medium is reported in this paper, for which comparative study of four population-based optimization algorithms are conducted. The method of finite difference time domain (FDTD) is employed for the analysis of the forward scattering part, while the inverse scattering problem is transformed into an optimization one. Four algorithms including particle swarm optimization (PSO), asynchronous particle swarm optimization (APSO), differential evolution (DE) and dynamic differential evolution (DDE) are applied to reconstruct the location and shape of a 2-D perfectly conducting cylinder. The performance of these optimization techniques is tested through the use of simulated fields to mimic the experimental measurements contaminated with additive white Gaussian noise. The reconstructed results show that DDE and APSO algorithms outperform the algorithms DE and PSO in terms of convergence speed. And DDE is concluded as the best algorithm in this study.

Index Terms - Inverse Scattering, Time Domain, FDTD, Sub-Grid Finite Difference Time Domain, Dynamic Differential Evolution, Asynchronous Particle Swarm Optimization, Slab Medium, Cubic Spline.

I. INTRODUCTION

The detection and reconstruction of certain buried and inaccessible scatterers by inverting microwave electromagnetic measurements is a research field of considerable interests because of its numerous applications in geophysical prospecting, civil engineering, and nondestructive testing. Numerical inverse scattering studies found in the literature are based on either frequency or time domain approaches [1]-[10]. However, it is well known that one major difficulty in inverse scattering problems is due to its ill-posedness in nature [11].

Another issue with inverse scattering problem is related to the nonlinearity because the inverting procedure involves the product of two unknowns: the electrical property of the object, and the electric field within the object. Especially, in the inverse problem involved with a dielectric slab medium there exists the interaction between the interfaces of three layers and the object, which leads to the complicated Green's function for this three-layer structure. Owing to the difficulties in computing the Green's function by numerical methods, the problems of inverse scattering involved with a dielectric slab were treated less intensively. In general, the nonlinearity of the problem is coped with by applying iterative optimization techniques [12]-[13].

The algorithms based on stochastic strategies offer advantages, over traditional deterministic

Submitted On: May 23, 2011
Accepted On: July 22, 2012

algorithms, which include strong search ability simplicity, robustness, and insensitivity to ill-posedness. In contrast to traditional deterministic methods, evolutionary searching schemes provide a more robust and efficient approach for solving inverse scattering problems. PSO and DE both work with a population of solutions; PSO is very efficient at exploring the entire search space, while DE is able to accomplish the same goal as genetic algorithm (GA) in a new and faster way. Thus several improved versions such APSO and DDE have gained considerable attention [14]-[19].

Time domain inverse scattering problems appear quite a lot in the area of remote sensing. Various time domain approaches had been proposed such as the layer-stripping approach [20], Born iterative method (BIM) [21], distorted Born iterative method (DBIM) [22] and different optimization approaches [23], [24]. The inverse scattering problems are usually treated by the traditional deterministic methods which are based on functional minimization via some gradient-type scheme. Furthermore, for gradient-type methods, it is well known that the convergence of the iteration depends highly on the initial guess. If a good initial guess is given, the speed of the convergence can be very fast. On the other hand, if the initial guess is far away from the exact one, the searching tends to get fail [25]. In general, they tend to get trapped in local minima when the initial trial solution is far away from the exact one. Thus, some population-based stochastic methods, such as GA [26], [27] PSO [28]-[31], DDE [32]-[34] are proposed to search the global extrema of the inverse problems to overcome the drawback of the deterministic methods.

Concerning the shape reconstruction of conducting scatterers, the PSO has been investigated whereas the steady-state genetic algorithm (SSGA) has been utilized in the reconstruction of metallic scatterers [27]. In this case, the reported results indicate that PSO is a reliable tool for inverse scattering application. Moreover, it has been shown that both DE and PSO outperform real-coded GA in terms of convergence speed [35], [36]. In recent decades, some papers have compared different algorithms for inverse scattering problems [14], [31], [37], [38]. However, to our knowledge, a comparative study about the performances of DDE and APSO mainly when applied to inverse scattering problems has not yet been investigated.

In this paper, the shape reconstruction is based on the application of DDE and APSO mainly. The forward problem is solved by the FDTD method, for which the sub-grid technique [39] is implemented to closely describe the fine structure of the cylinder. The inverse problem is formulated into an optimization one, and then the global searching schemes DE, DDE, PSO and APSO are used to search the parameter space. Cubic spline interpolation technique [40] is employed to reduce the number of parameters needed to closely describe a cylinder of arbitrary shape as compared to the Fourier series expansion.

The cost function of the four algorithms is to minimize the discrepancy between the simulated field (mimicking the measured one) and the estimated scattered field data with respect to the parameters of the cubic-spline expansion. Numerical results show that DDE outperforms APSO slightly in terms of shape reconstruction accuracy, giving a lower reconstruction error for the same number of iterations. As a whole, DDE and APSO algorithms outperform the algorithms DE and PSO in terms of convergence speed.

In section II, the details of the sub-grid FDTD method for the forward scattering are presented. In section III and IV, inverse problem and the numerical results of the proposed study are given, respectively. Finally, in section V some conclusions are drawn.

II. FORWARD PROBLEM

Let us consider a two-dimensional three-layer structure with the electromagnetic property (ε_1, μ_1) for region 1, (ε_2, μ_2) for region 2 and (ε_1, μ_1) for region 3, as shown in Fig. 1. A perfectly conducting cylinder to be de-embedded is buried in the second layer, and is parallel to z axis. The perfectly conducting cylinder is illuminated by a line source with Gaussian pulse shape placed at two different positions sequentially denoted by Tx in the first layer, and then the scattered *E* fields are recorded simultaneously at those points denoted by Rx in the same layer. The cross-section shape of the object is starlike and can be represented in polar coordinates with respect to the origin (X_O, Y_O) of the local coordinate in x-y plane as

shown in Fig. 2. The computational domain is discretized by using Yee cells [41]. It should be mentioned that the computational domain is surrounded by some optimized absorber of the perfect matching layer (PML) [42] to reduce the reflection from the surrounding PML environment.

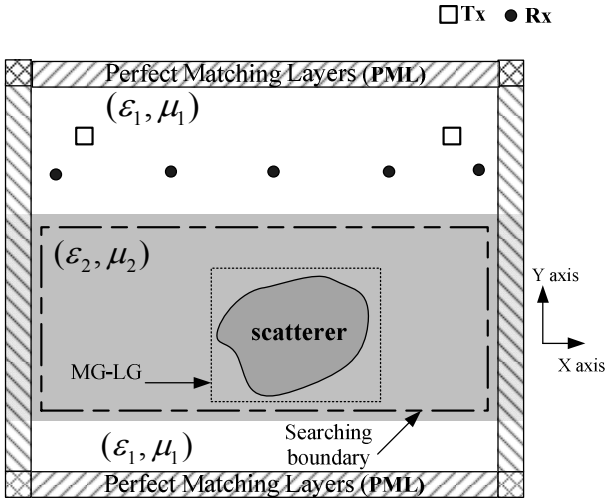

Fig. 1. Geometrical configuration of the problem.

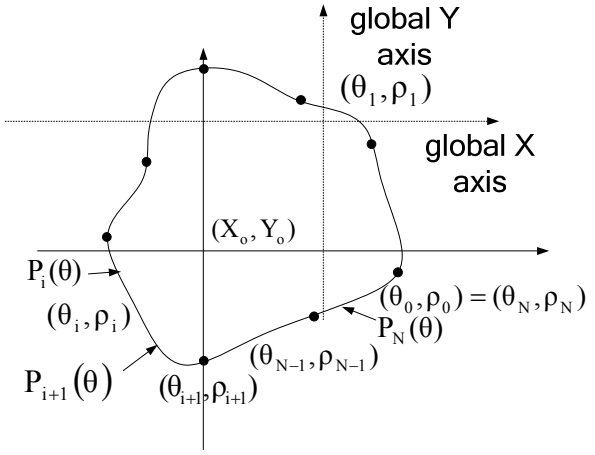

Fig. 2. A cylinder of arbitrary shape is described in terms of a closed cubic spline. The cubic spline consists of the polynomials of degree 3. (X_O, Y_O) is the center position in the x-y plane. The $\rho_1, \rho_2, \cdots, \rho_N$ are radius parameters to describe cylinder.

The direct scattering problem is to calculate the scattered electric fields while the shape and location of the scatterer are given. The shape function $F(\theta)$ of the scatterer is described by the trigonometric series in the direct scattering problem

$$F(\theta) = \sum_{n=0}^{N/2} B_n \cos(n\theta) + \sum_{n=1}^{N/2} C_n \sin(n\theta) \tag{1}$$

where *Bn* and *Cn* are real coefficients to expand the shape function.

In order to closely describe the shape of the cylinder for both the forward and inverse scattering procedure, the sub-grid technique is implemented in the FDTD code; the details are presented next.

The FDTD method is a direct implementation of the time-dependent Maxwell equations, written in finite-difference form for implementation on a computer.

$$\nabla \times \bar{E}(r,t) = -\frac{\partial \bar{B}(r,t)}{\partial t} \tag{2}$$

$$\nabla \times \bar{H}(r,t) = \frac{\partial \bar{D}(r,t)}{\partial t} + \bar{J}(r,t) \tag{3}$$

The finite-difference procedure was first proposed by Yee [41], who positioned the *E* and *H* fields at half-step intervals around a unit cell. Moreover, the *E* and *H* fields are evaluated at alternate half time steps, effectively through the use of centered difference expressions for both the space and time derivatives. The above equations can be easily implemented on a computer as follows:

$$E_z\Big|_{i+\frac{1}{2},j+\frac{1}{2}}^{n+1} = C_a\Big|_{i+\frac{1}{2},j+\frac{1}{2}} E_z\Big|_{i+\frac{1}{2},j+\frac{1}{2}}^{n} + C_b\Big|_{i+\frac{1}{2},j+\frac{1}{2}} \left[\frac{H_y\Big|_{i+1,j+\frac{1}{2}}^{n+\frac{1}{2}} - H_y\Big|_{i,j+\frac{1}{2}}^{n+\frac{1}{2}}}{\Delta x} \frac{H_x\Big|_{i+\frac{1}{2},j+1}^{n+\frac{1}{2}} - H_x\Big|_{i+\frac{1}{2},j}^{n+\frac{1}{2}}}{\Delta y} \right] \tag{4}$$

$$H_x\Big|_{i+\frac{1}{2},j}^{n+\frac{1}{2}} = H_x\Big|_{i+\frac{1}{2},j}^{n-\frac{1}{2}} - D\Big|_{i+\frac{1}{2},j} \left[\frac{E_z\Big|_{i+\frac{1}{2},j+\frac{1}{2}}^{n} - E_z\Big|_{i+\frac{1}{2},j-\frac{1}{2}}^{n}}{\Delta y} \right] \tag{5}$$

$$H_y\Big|_{i,j+\frac{1}{2}}^{n+\frac{1}{2}} = H_y\Big|_{i,j+\frac{1}{2}}^{n-\frac{1}{2}} - D\Big|_{i,j+\frac{1}{2}} \left[\frac{E_z\Big|_{i+\frac{1}{2},j+\frac{1}{2}}^{n} - E_z\Big|_{i-\frac{1}{2},j+\frac{1}{2}}^{n}}{\Delta x} \right] \tag{6}$$

$$C_a = \frac{1-\sigma\Delta t/2\varepsilon}{1+\sigma\Delta t/2\varepsilon} \quad C_b = \frac{\Delta t/\varepsilon}{1+\sigma\Delta t/2\varepsilon} \quad D = \Delta t/\varepsilon$$

Note that for nonmagnetic materials D is a constant.

In Fig. 3, *E* and *H* stand for the electric and magnetic fields on the major grids, respectively, while e and *h* denote the electric and magnetic fields on the local grids. If the scaling ratio is set at odd ratio, for example $1:3$, the *E* and *H* fields

coincide with *e* and *h* fields in the fine region as shown in Fig. 3. Note that the e and h fields inside the fine region can be updated through the normal Yee-cell algorithm [41] except those at the main-grid-local-grid (MG-LG) boundary [43], such as h_1, h_2 and h_3 in Fig. 3.

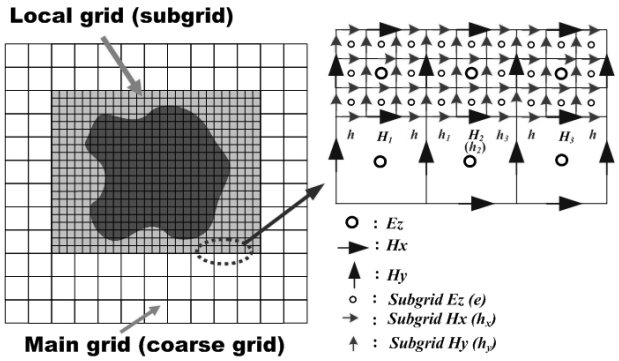

Fig. 3. Structure of the TM_z finite difference time domain method (FDTD) major grids and local grids for the scaling ratio (1:3), H fields are aligned with the main-grid-local-grid (MG-LG) boundary.

The *h* fields at the MG-LG interface can be linearly interpolated as follows :

$$h_1^{n+v} = H_1^{n+v} + \tfrac{2}{3}\left(H_2^{n+v} - H_1^{n+v}\right)$$
$$h_2^{n+v} = H_2^{n+v} \quad \text{, for } v = \frac{1}{3},\ \frac{2}{3} \text{ and } \frac{3}{3}. \tag{7}$$
$$h_3^{n+v} = H_2^{n+v} + \tfrac{1}{3}\left(H_3^{n+v} - H_2^{n+v}\right)$$

Note that the H fields don't exist on the main grids actually for $v = \frac{1}{3}$ and $\frac{2}{3}$ and need extra parabolic interpolation calculation by

$$H^{n+v} = H^n + Av + \frac{Bv^2}{2} \tag{8}$$

with $A = \dfrac{H^{n+1} - H^{n-1}}{2}$

$$B = H^{n+1} - H^{n-1} - 2H^n$$

The corresponding flow chart for updating the EM fields in the fine region is shown in Fig. 4. Note that at the time step $n+\frac{3}{6}$ the $E^{n+\frac{1}{2}}$ fields on the main grids should be updated by the coincided $e^{n+\frac{3}{6}}$ fields on the local grids. Similarly, at the time step $n+\frac{6}{6}$ the H^{n+1} fields are updated by the coincided $h^{n+\frac{6}{6}}$ fields.

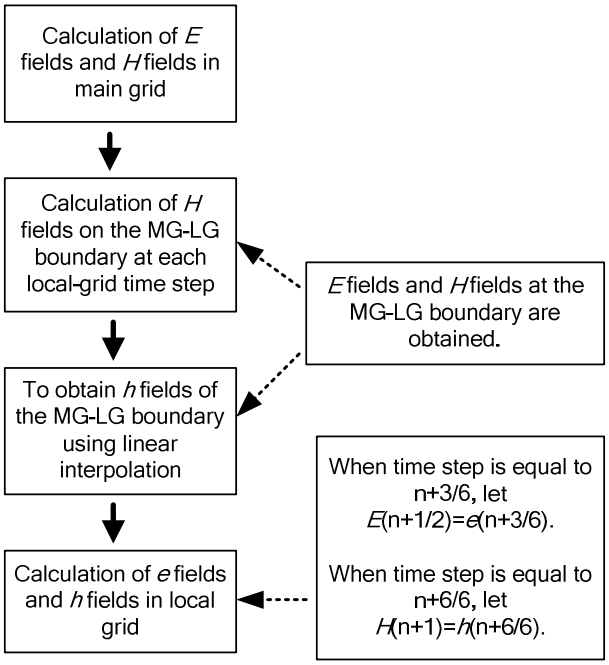

Fig. 4. The flowchart to update the (*E,H*) fields on the major grids and (*e*, *h*) fields on local grids.

For the time domain scattering and inverse scattering problems, the scatterer is assigned with the fine region such that the fine structure of the scatterer can be easily described. If higher resolution is needed, only the fine region needs to be rescaled using a higher ratio for sub-grid. This can avoid discretizing the whole problem space using the finest resolution such that the computational resources are utilized in a more efficient way, which is quite important for the computationally intensive inverse scattering problems. More details on the FDTD Sub-grid scheme can be found in [39].

III. INVERSE PROBLEM

For the inverse scattering problem, the shape and location of the metallic cylinder are reconstructed by the given scattered electric fields measured at the receivers, conceptually. The inverse problem is resolved by an optimization approach, for which the global searching DDE and APSO schemes, etc., are employed to minimize the following cost function (*CF*):

$$CF = \frac{\sum_{n=1}^{N_i}\sum_{m=1}^{M}\sum_{q=0}^{Q}\left|E_z^{exp}(n,m,q\Delta t) - E_z^{cal}(n,m,q\Delta t)\right|}{\sum_{n=1}^{N_i}\sum_{m=1}^{M}\sum_{q=0}^{Q}\left|E_z^{exp}(n,m,q\Delta t)\right|} \quad (9)$$

where E_z^{exp} and E_z^{cal} are the mimically experimental electric fields and the calculated electric fields, respectively. The N_i and M are the total number of the transmitters and receivers, respectively. Q is the total time step number of the recorded electric fields. The details of the proposed DE, DDE, PSO and APSO are presented next.

A. *Differential Evolution (DE) and Dynamic Differential Evolution (DDE)*

DE and DDE algorithms start with an initial population of potential solutions that is composed by a group of randomly generated individuals which represent the center position and the geometrical radii of the cylinders. The initial population may be expressed by $\{x_j : j = 1,\ 2, \cdots, Np\}$, where Np is the population size. Each individual in DE or DDE algorithms is a D-dimensional vector consisting of D parameters to be optimized. After initialization, DE and DDE algorithms perform the genetic evolution until the termination criterion is met. DE and DDE algorithms, like other evolutionary algorithms (EAs), also rely on the genetic operations (mutation, crossover and selection) to evolve generation by generation. The flowchart of the DDE algorithm is shown in Fig. 5. DE and DDE algorithms go through six procedures as follows:

1. Initialize a starting population: DE and DDE algorithms are initialized with a population that is composed by a group of randomly generated individuals. As mentioned above, individuals in DE and DDE algorithm represent a set of D-dimensional vectors in the parameter space for the problem, $\{x_j : j = 1,\ 2, \cdots, Np\}$, where D is the number of parameters to be optimized and Np is the population size.
2. Evaluate the population using cost function: After initialization, DE and DDE algorithms evaluate the cost function (9) for each individual in the population.

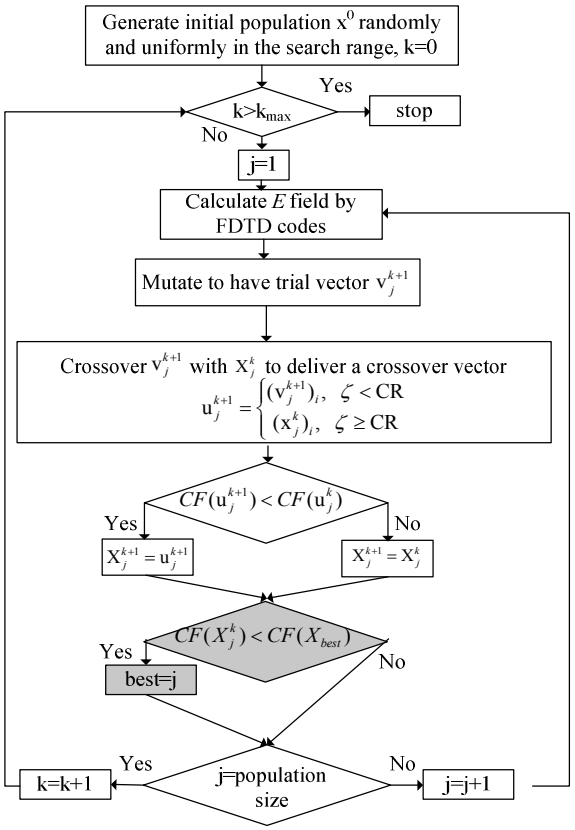

Fig. 5. Flowchart for the dynamic differential evolution. Pessimistic sub-area stands for dynamic update.

3. Perform mutation operation to generate trial vectors: The mutation operation of DDE algorithm is performed by arithmetical combination of individuals. A disturbing vector V_j^{k+1} is generated according to following equation:

$$(v_j^{k+1})_i = (x_j^k)_i + F\cdot[(x_{best}^k)_i - (x_j^k)_i] + \lambda\cdot[(x_m^k)_i - (x_n^k)_i]$$
$$, j = 0 \sim N_p - 1\ , m, n \in [0, N_p - 1]\ , \quad (10)$$
$$m \neq n\ ;\ i = 1 \sim D$$

where λ and F are the scaling factors associated with the vector differences $(x_{best}^k - x_j^k)$ and $(x_m^k - x_n^k)$, respectively. The disturbing vector v_j^{k+1} due to the mutation mechanism consists of parameter vector x_j^k, the best trial vector x_{best}^k and two randomly selected vectors x_m^k and

$\mathrm{x}_n^{\mathrm{k}}$. As comparison, the disturbing vector v_j^{k+1} is generated according to equation (11) for typical DE [12].

$$(\mathrm{v}_{\mathrm{j}}^{\mathrm{k+1}})_{\mathrm{i}} = (\mathrm{x}_{\mathrm{j}}^{\mathrm{k}})_{\mathrm{i}} + F \cdot [(\mathrm{x}_m^{\mathrm{k}})_{\mathrm{i}} - (\mathrm{x}_n^{\mathrm{k}})_{\mathrm{i}}] \ ,$$
$$j = 0 \sim N_p - 1, m, n \in [0, N_p - 1], \quad (11)$$
$$m \neq n \ ; \ i = 1 \sim D$$

where F are the scaling factors associated with the randomly selected vector difference $(\mathrm{x}_{\mathrm{m}}^{\mathrm{k}} - \mathrm{x}_{\mathrm{n}}^{\mathrm{k}})$. One of the main differences between DDE and DE is that DDE includes the idea of approaching the "Best" during the course of optimization procedure.

4. Perform crossover operation with probability of crossover CR to deliver crossover vectors: The crossover operation in DE and DDE algorithms is performed to increase the diversity of the parameter vectors. This operation is similar to the crossover process in GAs. However, the crossover operation in DE and DDE algorithms just allows delivering the crossover vector u_j^{k+1} by mixing the components of the current vector x_j^k and the disturbing vector V_j^{k+1}. It can be expressed as:

$$(\mathrm{u}_j^{k+1})_i = \begin{cases} (\mathrm{v}_j^{k+1})_i, & \zeta < \mathrm{CR} \\ (\mathrm{x}_j^k)_i, & \zeta \geq \mathrm{CR} \end{cases},$$
$$j = 0 \sim N_p - 1, i = 1 \sim D \quad (12)$$

where CR is the probability of crossover, $\mathrm{CR} \in (0,1)$. ζ is the random number generated uniformly between 0 and 1.

5. Perform selection operation to produce offspring: Selection operation is conducted by comparing the parent vector $\mathrm{x}_{\mathrm{j}}^{\mathrm{k}}$ with the crossover vectors $\mathrm{u}_{\mathrm{j}}^{\mathrm{k+1}}$. The vector with smaller cost function value is selected as a member of the next generation. Explicitly, the selection operation for the minimization problem is given by:

$$\mathrm{x}_j^{k+1} = \begin{cases} \mathrm{u}_j^{k+1} & , \text{if } \mathrm{CF}(\mathrm{u}_j^{k+1}) < \mathrm{CF}(\mathrm{x}_j^k) \\ \mathrm{x}_j^k & , \text{otherwise} \end{cases}$$
$$, j = 0 \sim N_p - 1 \quad (13)$$

Another major difference between DDE and DE is that DDE algorithm is carried out in a dynamic way: each parent individual would be replaced by its offspring if the offspring has yielded a better cost function value than its parent. While in a typical DE, all the updating actions of the population are performed at the end of the generation, for which it is referred to as static updating mechanism.

6. Stop the process and obtain the best individual if the termination criterion is satisfied, otherwise go to step 2.

Having realized the ideas of approaching the "Best" and dynamic updating, DDE thus exhibits better searching capability than DE does regarding the convergence speed. Hence, DDE is able to reduce the numbers of cost function evaluation and reconstruct the microwave image efficiently.

B. *The modified asynchronous Particle swarm optimization (APSO)*

Particle swarm global optimization is a class of derivative-free, population-based and self-adaptive search optimization technique which was introduced by Kennedy and Eberhart [13]. Particles (potential solutions) are distributed throughout the searching space and their positions and velocities are modified based on social behavior. The social behaviors in PSO exhibit a population of particles moving toward the most promising region of the search space. Clerc [44] proposed the constriction factor to adjust the velocity of the particle for obtaining the better convergence; the algorithm was named as constriction factor method (CFM). PSO starts with an initial population of potential solutions that is randomly generated and composed of N_p individuals (also called particles), of which each represents the location and the geometrical radii of the cylinder in this study.

After the initialization step, each particle of population is associated with a randomized velocity and position. Thus, each particle has a position and velocity vector, and can move through the problem space. In each generation, every particle changes its velocity according to its

best position up to date with the latest evolution, called x_{pbest} and the best particle in the swarm, called x_{gbest} .

Assume there are N_p particles in the swarm that is in a search space of D dimensions, the position and velocity of the j-th particle is determined according to the following equations according to the constriction factor method:

$$(v_j^{k+1})_i = \chi \cdot \begin{pmatrix} (v_j^k)_i + c_1 \cdot \phi_1 \cdot \left((x_{pbest,j})_i - (x_j^k)_i \right) \\ + c_2 \cdot \phi_2 \cdot \left((x_{gbest,j})_i - (x_j^k)_i \right) \end{pmatrix}$$

$$, j = 0 \sim N_p - 1,\ i = 1 \sim D \quad (14)$$

$$x_j^{k+1} = x_j^k + v_j^{k+1},\ j = 0 \sim N_p - 1,$$

$$i = 1 \sim D \quad (15)$$

where $\chi = \dfrac{2}{\left| 2 - \varphi - \sqrt{\varphi^2 - 4\varphi} \right|}$, $\varphi = c_1 + c_2 \geq 4$.

c_1 and c_2 are the learning coefficients used to control the impact of the local and global component in velocity equation (14). φ is the constriction factor. ϕ_1 and ϕ_2 are both random numbers between 0 and 1. $(v_j^k)_i$ and $(x_j^k)_i$ are the velocity and position of i-th dimension of the j-th particle at the k-th generation. It should be mentioned that the V_{max} method is also applied to control the particle's searching velocity and to confine the particle within the search space [45]. The value of V_{max} is set to be half of X_{max}, where X_{max} is the upper limit of the search space. Note that the V_{max} and X_{max} are maximum velocity and maximum distance, respectively. As an extreme case, if the maximum velocity V_{max} is set to X_{max}, the exploration in the inverse scattering problem space is not limited. Occasionally, the particles may move out of the search space, which could be remedied by applying the boundary condition to draw the foul particles back to the normal space.

The key distinction between PSO and APSO is on the updating mechanism, damping boundary condition and mutation scheme. In a typical synchronous PSO, the algorithm updates the velocities and positions of all particles using equations (14) and (15) till the end of each generation. And then update the best positions x_{pbest} and x_{gbest} . Alternatively, the updating mechanism of the asynchronous PSO use the following rule: after the position movement of each particle the new best positions x_{pbest} and x_{gbest} will be updated and then used for next particle immediately if the cost function value for the new position is better than the best record up to date. In this way, the swarm reacts more quickly to speed up the convergence.

The "damping boundary condition" is proposed by Huang and Mohan [46] to ensure the particles move within the legal search space. In many practical optimization problems, the rough location of the global optimum is usually difficult to know in advance. It is therefore required to have a boundary condition that can offer a robust and consistent performance for the PSO technique regardless of the problem. When a particle tends to move outside the search space, the position of particle is re-located about the search boundary and its velocity is multiplied by a random number (between 0 and 1) and arranged in the reverse direction .

Mutation scheme is introduced in PSO and APSO algorithms to speed up the convergence when particles are all around the global optimum. The mutation scheme can also avoid premature convergences in the searching procedure and help x_{gbest} escape from local optimal positions, thus the robustness of the PSO and APSO algorithms is assured.

The flowchart of the modified asynchronous PSO (APSO) is shown in Fig. 6. APSO goes through seven procedures as follows:

1. Initialize a starting population: randomly generate a swarm of particles.
2. Calculate the E fields by a home-made FDTD code.
3. Evaluate the population using cost function: the APSO algorithm evaluates the cost function (9) for each individual in the population.
4. Find x_{pbest} and x_{gbest} .
5. Mutation scheme: the PSO algorithm has been shown to converge rapidly during the initial stages of a global

search, but when around the global optimum, the search can become very slow. For the reason, mutation scheme is introduced into APSO. As shown in Fig. 6, there is an additional competition between the x_{gbest} and $x_{gbest_{mu}}$. The current x_{gbest} will be replaced by the $x_{gbest\,mu}$ if the $x_{gbest\,mu}$ is better than the current x_{gbest}. The $x_{gbest\,mu}$ is generated by following way:

$$x_{gbest_{mu}} = \begin{cases} x_{gbest} - \phi_3 \cdot \left[c_3 - (c_3 - c_4) \cdot \dfrac{k}{k_{\max}} \right] \cdot \left(\mathrm{X}_{\max} - \mathrm{X}_{\min} \right), & if \quad \phi_{mu} < 0.5 \\ x_{gbest} + \phi_3 \cdot \left[c_3 - (c_3 - c_4) \cdot \dfrac{k}{k_{\max}} \right] \cdot \left(\mathrm{X}_{\max} - \mathrm{X}_{\min} \right), & if \quad \phi_{mu} \geq 0.5 \end{cases} \tag{16}$$

where c_3 and c_4 are the scaling parameter. ϕ_3 and ϕ_{mu} are both the random numbers between 0 and 1. k is the current iteration number. $k_{\max}$ is the maximum iteration number. $\mathrm{X}_{\max}$ and $\mathrm{X}_{\min}$ are the upper limit and lower limit of the search space, respectively.

6. Update the velocity and position.
7. Stop the process and obtain the best individual if the termination criterion is satisfied, otherwise, go to step 2.

It should be noted that since both APSO and DDE realize the ideas of approaching the "Best" and dynamic updating, they exhibit similar searching capability and convergence property.

B. *Cubic spline interpolation technique*

It should be noted that in the inverse problem, the shape function of the 2-D perfectly conducting cylinder is described by a cubic spline in this study instead of the trigonometric series (1) shown in the section of the forward problem. The cubic spline is more efficient in terms of the unknown number required to describe a cylinder of arbitrary cross section. In addition, by using the cubic spline the coordinates of local origin inside the cylinder serve as the searching parameters and can move around the searching space, which is very hard to achieve, if not impossible, when the trigonometric series expansion is used in the inversion procedure. Thus by using the cubic spline expansion, the justification for the objective of the inverse scattering is maintained.

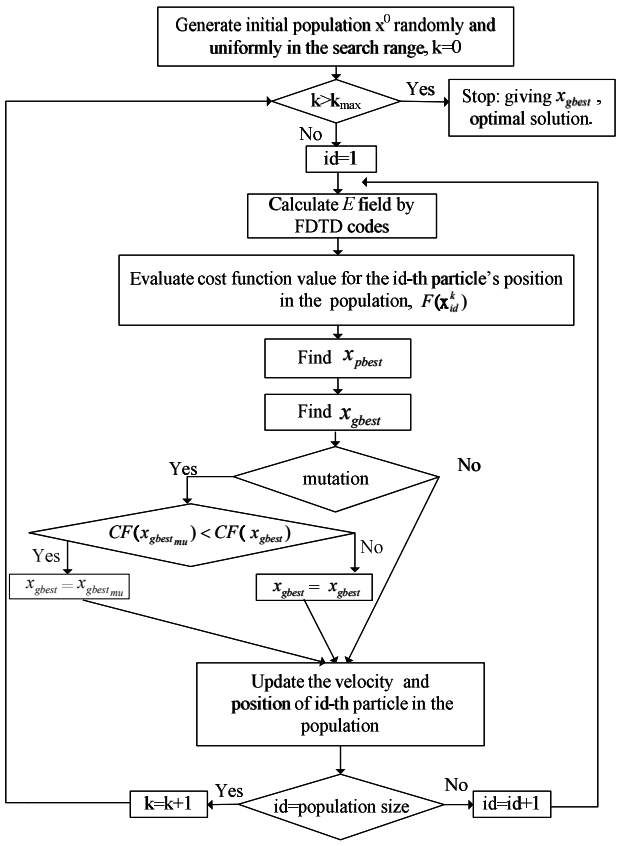

Fig. 6. Flowchart for the modified APSO.

As shown in Fig. 2, the cubic spline consists of the polynomials of degree 3 $P_i(\theta)$, $i = 1, 2, \cdots, N$, which satisfy the following smooth conditions:

$$\begin{aligned} P_i(\theta_i) = P_{i+1}(\theta_i) \equiv \rho_i \\ P_i'(\theta_i) = P_{i+1}'(\theta_i) \\ i = 1, 2, \cdots, N \\ P_i''(\theta_i) = P_{i+1}''(\theta_i) \end{aligned} \tag{17}$$

and

$$P_1(\theta_0) = P_N(\theta_N)$$
$$P_1'(\theta_0) = P_N'(\theta_N) \equiv \rho_N'$$
$$P_1''(\theta_0) = P_N''(\theta_N) \quad (18)$$

Through the interpolation of the cubic spline, an arbitrary smooth cylinder can be easily described through the radius parameters $\rho_1, \rho_2, \cdots, \rho_N$ and the slope ρ_N', of which the details are referred to [40]. By combining the PSO, APSO, DE or DDE algorithm with the cubic spline interpolation technique, together with the FDTD sub-grid method, we are able to reconstruct the microwave image efficiently.

It should be noted that the coordinates of local origin inside the cylinder plus the radii of the geometrical spline used to describe the shape of the cylinder will be determined by the PSO, APSO, DE and DDE algorithms.

IV. NUMERICAL RESULTS

As shown in Fig. 1, the problem space is divided in 68×68 grids with the grid size $\Delta x = \Delta y$ =5.95 mm. The metallic cylinder is buried in a lossless slab medium ($\sigma_1 = \sigma_2 = \sigma_3 = 0$). The transmitters and receivers are placed in free space above the homogeneous dielectric. The permittivities in regions 1, 2 and 3 are characterized by $\varepsilon_1 = \varepsilon_0$, $\varepsilon_2 = 8\varepsilon_0$ and $\varepsilon_3 = \varepsilon_0$, respectively, while the permeability μ_0 is used for each region; i.e., only non-magnetic media are concerned here.

The scatterer is illuminated by cylindrical waves with the electric field polarized along the z axis, while the time dependence of the field is a derivative Gaussian pulse. The waveform is plotted in Fig. 7. The cylindrical object is illuminated by a transmitter at two different positions (N_i=2), which are located at (-143mm, 178.5mm) and (143mm, 178.5mm), respectively. The scattered E fields for each illumination are collected at the five receivers (M=5), which are equally separated by 47.8mm along the line at distance 48mm from the interface between region 1 and region 2.

The time duration is set to $300\,\Delta t$ ($q = 300$). In order to describe the shape of the cylinder more accurately, the sub-grid FDTD technique is employed both in the forward scattering (1:9) and the inverse scattering (1:5) - but with different scaling ratios as indicated in the parentheses. The proposed inversion procedures are implemented through some home-made Fortran programs that runs on an Intel PC (3.4 GHz/ 2G memory /500 G). The typical CPU time needed for DDE and APSO examples are about 11 and 9.5 hours, respectively, in this study.

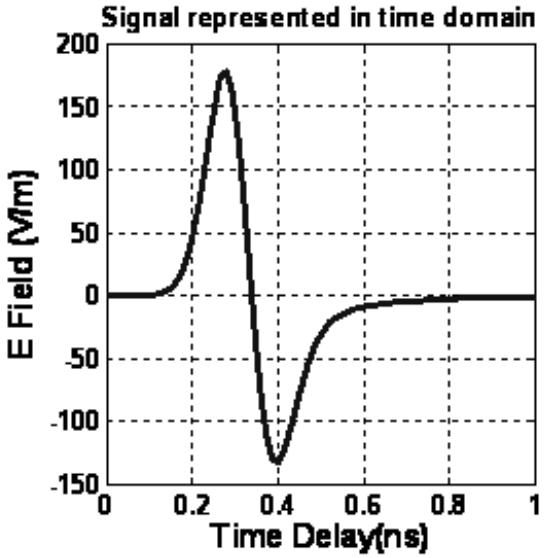

Fig. 7. Signal represented in time domain.

Three examples are investigated for the inverse scattering of the proposed structure by using the DDE and APSO, etc. There are eleven unknown parameters to retrieve, which include the center position (X_o, Y_o), the radius ρ_i, $i = 1, 2, \cdots, 8$ of the shape function and the slope ρ_N'. Relatively wide searching ranges are used for DDE and APSO, etc, to optimize the cost function given by (9). The parameters and the corresponding searching ranges are listed as follows: $-47.6\text{mm} \le X_o \le 47.6\text{mm}$, $-47.6\text{mm} \le Y_o \le 47.6\text{mm}$, $5.95\text{mm} \le \rho_i \le 71.4\text{mm}$, $i = 1, 2, \cdots, 8$, $-1 \le \rho_N' \le 1$. The operational coefficients for the DDE algorithm are set as below: The crossover rate CR=0.8. The weighting factor $F = \lambda$=0.8 and the population size Np=110.

The relative coefficients of the modified APSO are set below. The learning coefficients c_1 and c_2 are set to 2.8 and 1.3, respectively. The scaling parameter, c_3 and c_4 , are set to 0.1 and 0.05, respectively. The mutation probability is 0.4 and the population size is set to 30. Here, the shape error *DF* is defined as

$$DF = \{\frac{1}{N'}\sum_{i=1}^{N'}[F^{cal}(\theta_i) - F(\theta_i)]^2 / F^2(\theta_i)\}^{1/2} \quad (19)$$

where the N' is set to 720.

As mentioned above, application of sub-grid technique can result in large savings of computer time and memory for the FDTD method. Thus, in this study, sub-grid FDTD technique is implemented to efficiently describe the details of the dielectric cylinders shape. For the first example, the perfectly conducting cylinder with shape function $F(\theta) = 29.75$ (unit: mm) is tested. In Figs. 8 and 9, the standard FDTD with uniform grid of (1:1) case is compared with the sub-grid FDTD cases of different scaling ratios (1:3), (1:5) and (1:7) for the inverse scattering by DDE and APSO algorithms, respectively. The reconstructed details are listed in Table I for DDE and APSO algorithms, respectively. Obviously, the results obtained by using the standard FDTD with uniform grid (1:1) are not as good as those of the sub-grid FDTD cases. Moreover, the values of *DF* for DDE and APSO algorithms are very close.

Table 1: The errors of the reconstructed shape function for example 1 by using different subgridding ratios.

subgridding ratio	DF via DDE	DFvia APSO
1:1	9.38%	8.92%
1:3	1.85%	4.50%
1:5	1.35%	1.68%
1:7	1.02%	1.52%

It also suggests that the scaling ratio (1:5) is suitable for the following examples to be studied. On the other hand, in order to achieve the same accuracy for the standard FDTD with uniform grid, the grid size of the whole space has to be reduced to smoothly describe the geometry of the perfectly conducting cylinder, however, the computation time would be increased quite a lot, 3.85 times as compared to the subgrid FDTD scheme of (1:5) case. Moreover, the convergence curves of the cost function versus generation as the proposed DDE and APSO algorithms being executed five times out of ten by using different random seeds are shown in Figs. 10 and 11, respectively to demonstrate the stability of the algorithms.

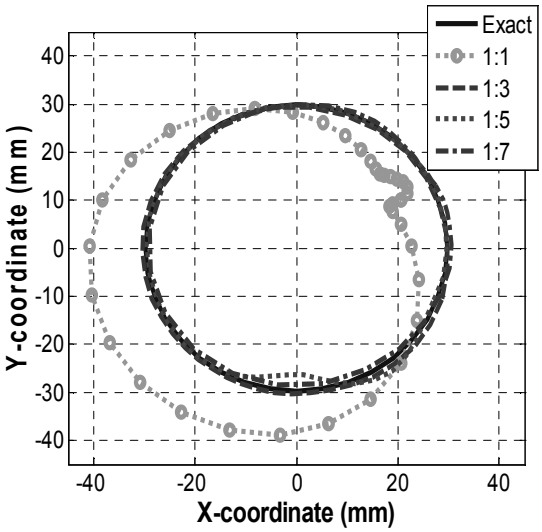

Fig. 8. The reconstructed shapes of the cylinder for example 1 by using different scaling ratios for the sub-grid via DDE. The shape function of this object is given by $F(\theta) = 29.75$ mm.

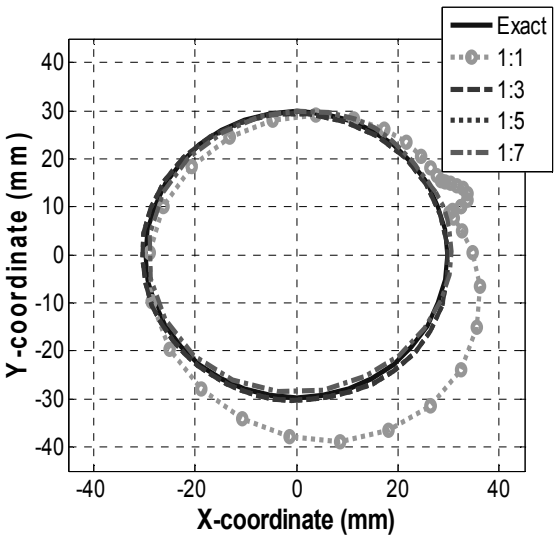

Fig. 9. The reconstructed shapes of the cylinder for example 1 by using different scaling ratios for the sub-grid via APSO.The shape function of this object is given by $F(\theta) = 29.75$ mm.

For the second example, a non-symmetric perfectly conducting cylinder with shape function $F(\theta)=29.75+11.9\cos(2\theta)+5.95\sin(\theta)+5.95\sin(2\theta)$ (unit:mm) is considered. Figure 12 shows the reconstructed images by of the use of DDE, APSO, DE and PSO algorithms for comparison. The values of DF for DDE, APSO, DE and PSO are about 5.8%, 11.4%, 17.9% and 25.3% in the final generation, respectively. The cost function value versus the number of function call is shown in Fig. 13. PSO is severely affected by premature convergence and stagnation problem. The key differences between PSO and APSO are about the convergence speed, the computation time and the accuracy, since APSO includes damping boundary condition scheme and mutation scheme. The performance of DDE is the best in this example.

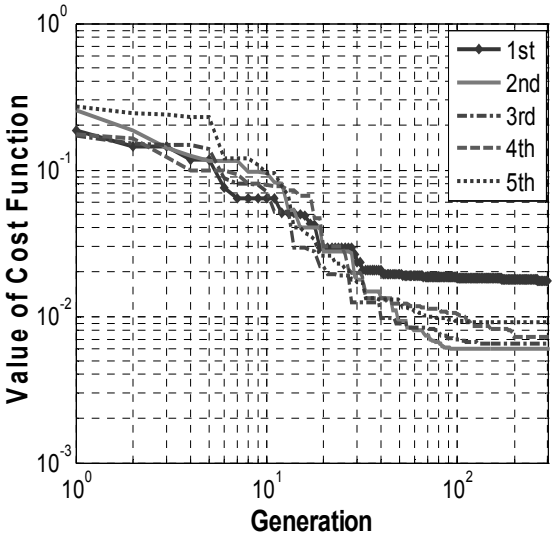

Fig. 10. The convergence curves of the cost function versus generation as the proposed DDE algorithm being executed five times out of ten by using different tables of random number.

In order to investigate the sensitivity of the imaging algorithm against random noise, the mimical experimental scattered fields are then contaminated by white Gaussian noise of zero mean. The relative noise level (RNL) is defined as:

$$RNL=\frac{\sigma_g}{\sqrt{\dfrac{\sum_{n=1}^{N_i}\sum_{m=1}^{M_i}\sum_{k=0}^{K}\left|E_z^{\exp}(n,m,k\Delta t)\right|^2}{(N_i)(M_i)(K+1)}}} \quad (20)$$

The relative noise levels of 10^{-4}, 10^{-3}, 10^{-2}, 0.1 and 0.5 are tested. Figure 14 shows the values of DF of the final reconstructed results vs. RNL. It is observed that good reconstruction can be achieved regarding the shape of the metallic cylinder when the relative noise level is below 10^{-2}.

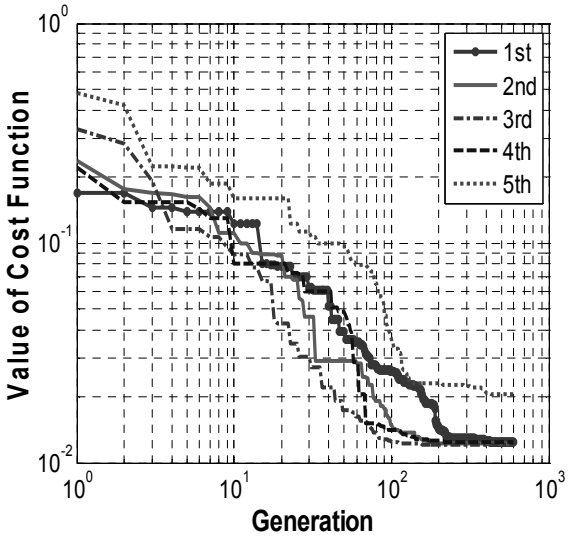

Fig. 11. The convergence curves of the cost function versus generation as the proposed APSO being executed five times out of ten by using different tables of random number.

For the third example, the shape function of this object is given by $F(\theta)=29.75+5.95\cos(3\theta)$ (unit:mm) is considered. Figure 15 shows that the reconstructed images by of the use of DDE, APSO, DE and PSO algorithms for comparison. The values of DF for DDE, APSO, DE and PSO are about 5.3%, 9.6%, 14.3% and 19.6% in the final generation, respectively. Figure 16 shows that the cost function versus the number of function call. It is clear that the DDE and APSO outperform PSO. The latter PSO is severely affected by premature convergence and/or stagnation problem, while the former DDE and APSO are more robust to avoid local optimal due to the inclusion of dynamic update and/or the "Best" concept for optimization as mentioned previously [32]-[34].

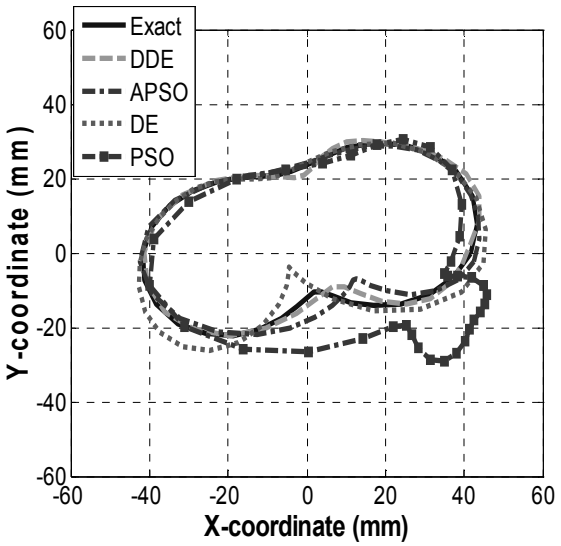

Fig. 12. The reconstructed cross section of the cylinder of example 2 by DDE, APSO, DE and PSO. The shape function of this object is given by $F(\theta)=29.75+11.9\cos(2\theta)+5.95\sin(\theta)+5.95\sin(2\theta)$ mm.

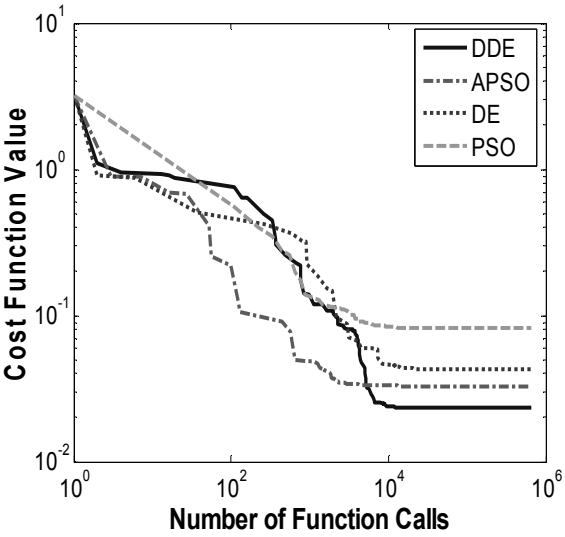

Fig. 13. The value of cost function versus the number of function call for example 2. The shape function of this object is given by $F(\theta)=29.75+11.9\cos(2\theta)+5.95\sin(\theta)+5.95\sin(2\theta)$ mm.

Again, investigation on the sensitivity of the imaging algorithms against random noise is conducted for this example. Figure 17 shows the values of DF of the final reconstructed results vs. RNL. It could be observed that good reconstruction can be achieved regarding the shape of the metallic cylinder when the relative noise level is below 10^{-2}. It is worth to mention that the image reconstruction at the backside of the scatterer is relative hard due to the shadowing effect in example 3.

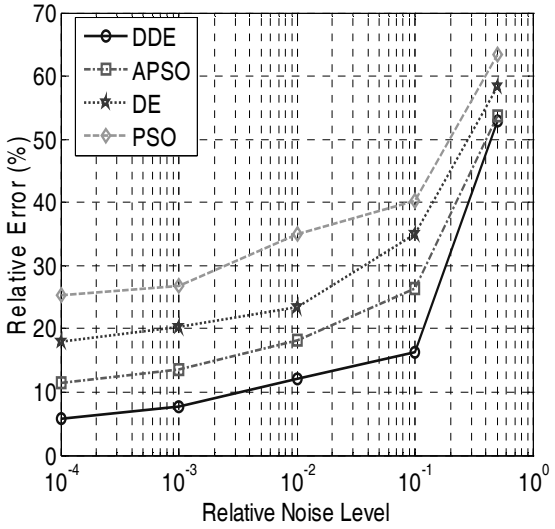

Fig. 14. Shape error as function of RNL by DDE, APSO, DE and PSO, respectively. The shape function of this object is given by $F(\theta)=29.75+11.9\cos(2\theta)+5.95\sin(\theta)+5.95\sin(2\theta)$ mm.

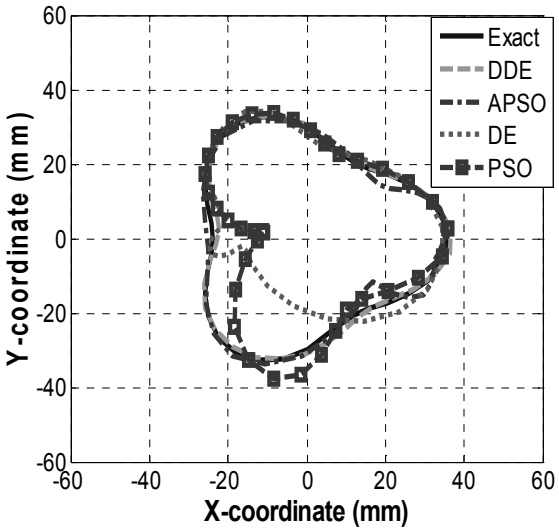

Fig. 15. The reconstructed cross section of the cylinder of example 3 by DDE, APSO, DE and PSO. The shape function of this object is given by $F(\theta)=29.75+17.85\cos(3\theta)$ mm.

Finally, the computational burden, which is related to the generation of new solution candidates from the previous ones, is roughly the same for DDE and APSO. For the shape reconstruction examples studied, the computation

time is dominated by the FDTD procedure of the direct-scattering problems.

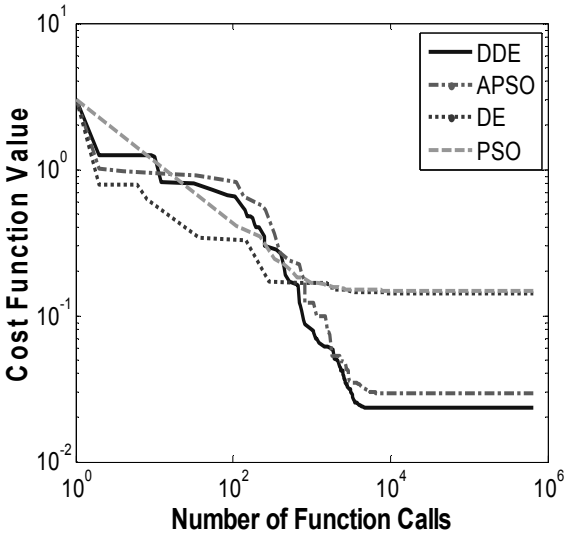

Fig. 16. The value of cost function versus the number of function call for example 2. The shape function of this object is given by $F(\theta) = 29.75 + 17.85\cos(3\theta)$ mm.

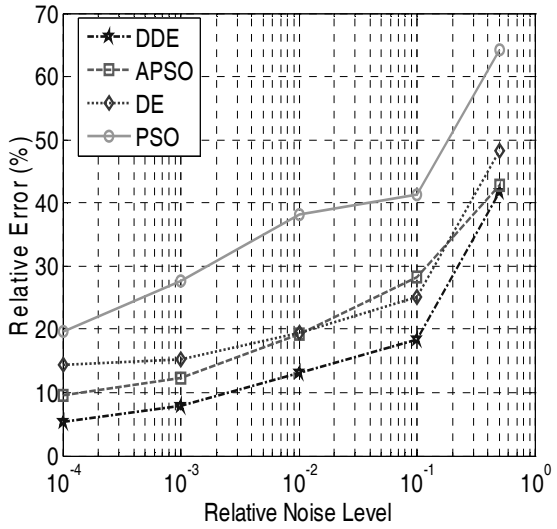

Fig. 17. Shape error as function of RNL by DDE, APSO, DE and PSO, respectively. The shape function of this object is given by $F(\theta) = 29.75 + 17.85\cos(3\theta)$ mm.

V. CONCLUSION

The problem of shape reconstruction of perfectly conducting cylinder is investigated by applying DDE, APSO DE and PSO techniques, for which the inverse problem is reformulated into an optimization one. Since both DDE and APSO realize the ideas of approaching the "Best" and dynamic updating, they exhibit similar searching capability and convergence property and outperform DE and PSO. Numerical results show that DDE and APSO are reliable for the time domain inverse problem of 2D metallic cylinder even when the initial guess is far from the exact one. Moreover, DDE and APSO can result in accurate reconstruction even when the effects of noise are included under the condition of noise level less than 10^{-2}. It should be mentioned that this comparative study is indicative and its conclusion should not be considered generally applicable in all inverse scattering problems.

ACKNOWLEDGMENT

This work was supported by National Science Council, Republic of China, under Grant NSC 101-2221-E-229-001.

REFERENCES

[1] C. H. Huang, C. C. Chiu, C. J. Lin, Y. F. Chen, "Inverse Scattering of Inhomogeneous Dielectric Cylinders Buried in a Slab Medium by TE Wave Illumination," *Applied Computational Electromagnetics Society (ACES) Journal*, vol. 22, no. 2, pp. 295 - 301, July 2007.

[2] G. Oliveri, P. Rocca, and A. Massa, "A Bayesian Compressive Sampling-based Inversion for Imaging Sparse Scatterers," *IEEE Transactions on Geosciences and Remote Sensing*, vol. 49, no. 10, pp. 3993-4006, October, 2011.

[3] L. Poli, G. Oliveri, and A. Massa, "Microwave Imaging within the First-order Born Approximation by means of the Contrast-field Bayesian Compressive Sensing," *IEEE Transactions on Antennas and Propagation*, vol. 60, no. 6, pp. 2865-2879, Jun. 2012.

[4] L. Pan, Y. Zhong, X. Chen and S. P. Yeo "Subspace-Based Optimization Method for Inverse Scattering Problems Utilizing Phaseless Data," *IEEE Transactions Geoscience and Remote Sensing,* vol. 49, no. 3, pp. 981 - 987, Mar. 2011

[5] I. Jeffrey, V. I. Okhmatovski, J. LoVetri, C. Gilmore, "An Adaptive Basis Function Solution to the 1D and 2D Inverse Scattering Problems using the DBIM and the BIM," *Applied Computational Electromagnetics Society (ACES) Journal*, vol. 22, no. 1, pp. 60-70, March 2007.

[6] C. Loo, M. Hamid, "Inverse Scattering of a Dielectric Sphere Partially Buried in a Ground Plane Using a Radial Basis Function Network," *Applied Computational Electromagnetics Society (ACES) Journal*, vol. 19, no. 3, pp. 135-146, November 2004.

[7] C. H. Sun, C. C. Chiu, and C. J. Lin "Image Reconstruction of Inhomogeneous Biaxial Dielectric Cylinders Buried in a Slab Medium.", *International Journal of Applied Electromagnetics and Mechanics*, vol. 34, no.1, 2, pp. 33-48, Nov. 2010.

[8] C. H. Sun and C. C. Chiu "Electromagnetic imaging of Buried Perfectly Conducting Cylinders Targets Using the Dynamic Differential Evolution." *International Journal of RF and Microwave Computer-Aided Engineering.* vol. 22, no 2, pp. 141-146, Mar. 2012.

[9] C. H. Sun, C. C. Chiu, and C. J. Lin "Image Reconstruction of Inhomogeneous Biaxial Dielectric Cylinders Buried in a Slab Medium." *International Journal of Applied Electromagnetics and Mechanics*, vol. 34, no.1, 2, pp. 33-48, Nov. 2010.

[10] W. Chien, C. H. Sun, C. C. Chiu, "Image Reconstruction for a Partially Immersed Imperfectly Conducting Cylinder by Genetic Algorithm," *International Journal of Imaging Systems and Technology* vol. 19, pp. 299-305, Dec. 2009.

[11] P. C. Sabatier, "Theoretical Considerations for Inverse Scattering," *Radio Science,* vol. 18, pp. 629 - 631, Jan. 1983.

[12] R. Storn, and K. Price, "Differential Evolution - a Simple and Efficient Adaptive Scheme for Global Optimization over Continuous Spaces," Technical Report TR-95-012, International Computer Science Institute, Berkeley, 1995.

[13] J. Kennedy and R. C. Eberhart, "Particle Swarm Optimization," *Proceedings of the IEEE International Conference on Neural Network*, pp. 1942-1948, 1995.

[14] I. T. Rekanos, "Shape Reconstruction of a Perfectly Conducting Scatterer Using Differential Evolution and Particle Swarm Optimization," *IEEE Transactions on Geoscience and Remote Sensing*, vol. 46, no. 7, pp. 1967-1974, 2008.

[15] A. Semnani and M. Kamyab, "An Enhanced Method for Inverse Scattering Problems Using Fourier Series Expansion in Conjunction with FDTD and PSO," *Progress In Electromagnetic Research.* PIER 76, pp. 45-64, 2007.

[16] M. Farmahini-Farahani, R. Faraji-Dana, M. Shahabadi, "Fast and Accurate Cascaded Particle Swarm Gradient Optimization Method for Solving 2-D Inverse Scattering Problems," *Applied Computational Electromagnetics Society (ACES) Journal*, vol. 24, no. 5, pp. 511-517, October 2009.

[17] C. H. Sun, C. L. Liu, K. C. Chen, C. C. Chiu, C. L. Li, and C. C. Tasi, "Electromagnetic Transverse Electric Wave Inverse Scattering of a Partially Immersed Conductor by Steady-State Genetic Algorithm," *Electromagnetics.* vol. 28, no. 6, pp. 389-400, Aug. 2008.

[18] W. Chien, C-C. Chiu, "Cubic-Spline Expansion with GA for Half-Space Inverse Problems," *Applied Computational Electromagnetics Society (ACES) Journal*, vol. 20, no. 2, pp. 136-143, July 2005.

[19] C. C. Chiu, C. H. Sun and Y. S. Fan "Shape Reconstruction of 2-D Perfectly Conducting Cylinder Targets Using the Particle Swarm Optimization." *Imaging Science Journal.* vol. 60, no. 2, pp. 83-89, Apr. 2012.

[20] A. E. Yagle and J. L. Frolik, "On the Feasibility of Impulse Reflection Response Data for the Two-dimensional Inverse Scattering Problem," *IEEE Transactions on Antennas and Propagation.* vol. 44, no. 12, pp. 1551-1564, Dec. 1996.

[21] M. Moghaddam, W. C. Chew, and M. Oristaglio, "A Comparison of the Born Iterative Method and Tarantola's Method for an Electromagnetic Time-domain Inverse Problem," *International Journal of Imaging Systems and Technology*, vol. 3, pp. 318-333, 1991.

[22] W. H. Weedon, "*Broadband Microwave Inverse Scattering: Theory and Experiment*," Ph.D. dissertation, University of Illinois at Urbana-Champaign, 1994.

[23] I. T. Rekanos, "Time-domain Inverse Scattering using Lagrange Multipliers: an Iterative FDTD-based Optimization Technique," *Journal of Electromagnetic Waves and Applications*, vol. 17, no. 2, pp. 271-289, 2003.

[24] M. Benedetti, D. Lesselier, M. Lambert, and A. Massa, "A Multi-resolution Technique Based on Shape Optimization for the Reconstruction of Homogeneous Dielectric Objects," *Inverse Problems*, vol. 25, no. 1, pp. 1-26, January 2009.

[25] C. H. Huang, Y. F. Chen, and C. C. Chiu, "Permittivity Distribution Reconstruction of Dielectric Objects by a Cascaded Method," *Journal of Electromagnetic Waves and Applications* vol. 21, no. 2, pp. 145-159, Jan. 2007.

[26] C. H. Sun, C. L. Li, C. C. Chiu and C. H. Huang, "Time Domain Image Reconstruction for a Buried 2D Homogeneous Dielectric Cylinder Using NU-SSGA.", *Research in Nondestructive Evaluation,* vol. 22, no.1, pp. 1-15, Jan. 2011.

[27] C. H. Huang, C. C. Chiu, C. L. Li, and Y.-H. Li, "Image Reconstruction of the Buried Metallic Cylinder Using FDTD Method and SSGA," *Progress In Electromagnetic Research.* PIER 85, pp. 195-210, Aug. 2008.

[28] C. H. Huang, C. H. Chen, C. C. Chiu and C. L. Li, "Reconstruction of the Buried Homogenous

Dielectric Cylinder by FDTD and Asynchronous Particle Swarm Optimization." *Applied Computational Electromagnetics Society (ACES) Journal,* vol. 25, no. 8, pp. 672-681, Aug. 2010.

[29] C. H. Sun, C. C. Chiu and C. L. Li, "Time-Domain Inverse Scattering of a Two- dimensional Metallic Cylinder in Slab Medium Using Asynchronous Particle Swarm Optimization.", *Progress In Electromagnetic Research M.* (PIER M), vol. 14, pp. 85-100. Aug. 2010.

[30] A. Semnani, M. Kamyab, "An Enhanced Hybrid Method for Solving Inverse Scattering Problems," *IEEE Transactions on Magnetics*, vol. 45, no. 3, pp. 1534-1537, Mar. 2009.

[31] C. C. Chiu, C. H. Sun and W. L. Chang "Comparison of Particle Swarm Optimization and Asynchronous Particle Swarm Optimization for Inverse Scattering of a Two- Dimensional Perfectly Conducting Cylinder.", *International Journal of Applied Electromagnetics and Mechanics,* vol. 35, no.4, pp. 249-261, Apr. 2011.

[32] C. H. Sun, C. C. Chiu, C. L. Li, and C. H. Huang, "Time Domain Image Reconstruction for Homogenous Dielectric Objects by Dynamic Differential Evolution," *Electromagnetics.* vol. 30, no. 4, pp. 309-323, May 2010.

[33] C. H. Sun, C. C. Chiu, W. Chien and C. L. Li, "Application of FDTD and Dynamic Differential Evolution for Inverse Scattering of a Two-Dimensional Perfectly Conducting Cylinder in Slab Medium", *Journal of Electronic Imaging,* vol. 19, 043016, Dec. 2010.

[34] C. C. Chiu and C. H. Sun "A Study of Microwave Imaging for a Metallic Cylinder." *International Journal of RF and Microwave Computer-Aided Engineering*, vol. 22, no. 5, pp. 632-638, Sept. 2012.

[35] M. Donelli and A. Massa, "Computational Approach Based on a Particle Swarm Optimizer for Microwave Imaging of Two-dimensional Dielectric Scatterers," *IEEE Trans. Microw. Theory Tech.*, vol. 53, no. 5, pp. 1761-1776, May 2005.

[36] M. Donelli, G. Franceschini, A. Martini, and A. Massa, "An Integrated Multiscaling Strategy Based on a Particle Swarm Algorithm for Inverse Scattering Problems," *IEEE Trans. Geosci. Remote Sens.*, vol. 44, no. 2, pp. 298-312, Feb. 2006.

[37] C. C. Chiu and W. C. Hsiao "Comparison of Asynchronous Particle Swarm Optimization and Dynamic Differential Evolution for Partially Immersed Conductor." *Waves in Random and Complex Media.* vol. 21, no. 3, pp. 485-500, Aug. 2011.

[38] A. Semnani, M. Kamyab, and I. T. Rekanos, "Reconstruction of One-Dimensional Dielectric Scatterers Using Differential Evolution and Particle Swarm Optimization," *IEEE Geoscience and Remote Sensing Letters*, vol. 6, no. 4, pp. 671-675, Oct. 2009.

[39] M. W. Chevalier, R. J. Luebbers and V. P. Cable, "FDTD Local Grid with Material Traverse," *IEEE Trans. Antennas and Propagation*, vol. 45, no. 3, pp. 411-421, March 1997.

[40] C. de Boor, "*A Practical Guide to Splines*," Springer-Verlag, New York, 1978.

[41] K. Yee, "Numerical Solutions of Initial Boundary Value Problems involving Maxwell's Equations in Isotropic Media," *IEEE Transactions on Antennas and Propagation*, vol. AP-14, pp. 302-307, 1966.

[42] C. L. Li, C. W. Liu, and S. H. Chen, "Optimization of a PML Absorber's Conductivity Profile using FDTD," *Microwave and Optical Technology Leters.*, vol. 37, pp. 380-383, 2003.

[43] I. S. Kim and W. J. R. Hoefer, "A Local Mesh Refinement Algorithm for the Time-domain Finite-difference Method using Maxwell's Curl Equations," *IEEE Trans. Microwave Theory Tech.,* vol. 38, no. 6, pp. 812-815, June 1990.

[44] M. Clerc, "The Swarm and the Queen: Towards a Deterministic and Adaptive Particle Swarm Optimization," *Proceedings of Congress on Evolutionary Computation*, Washington, DC, pp. 1951-1957, 1999.

[45] A. Carlisle and G. Dozier, "An Off-The-Shelf PSO," *Proceedings of the 2001 Workshop on Particle Swarm Optimization*, pp. 1-6, 2001.

[46] T. Huang, A. S. Mohan, "A Hybrid Boundary Condition for Robust Particle Swarm. Optimization," *IEEE Antennas and Wireless Propagation Letters*, vol. 4, pp. 112-117, 2005.

Ching-Lieh Li was born November 24, 1963, in Pingtun, Taiwan. He received the B.S. degree from National Taiwan University, Taipei, Taiwan, in 1985, and the M.S. and Ph.D. degrees from Michigan State University, East Lansing, in 1990 and 1993, respectively, all in electrical engineering. From 1989 to 1993, he was a Research Assistant in the Electrical Engineering Department, Michigan State University, where he worked on the measurement techniques for determining the electromagnetic properties of materials. In 1993, he joined the Electrical Engineering Faculty at Tamkang University, Taipei, Taiwan, where now he is a professor. Currently, his research activities involve inverse scattering problem, and microstrip antenna design and dielectric material

characterization, etc.. His areas of special interest include theoretical and computational electromagnetics, and application of various optimization schemes such as SSGA, PSO, DE, and Taguchi method to electromagnetics.

Chung-Hsin Huang was born in New Taipei City, Taiwan, Republic of China, on February 1, 1980. He received M.S.E.E. and Ph.D degrees in electrical engineering from Tamkang University, Taipei, Taiwan, in 2004 and 2009 respectively. He is currently an Assistant Professor with the Department of Computer and Communication Engineering, Taipei College of Maritime Technology. His current research interests include electromagnetic wave theory and applications, optimization methods, dielectric material characterization and wireless communications.

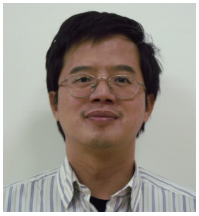

Chien-Ching Chiu received his BSCE degree from National Chiao Tung University, Hsinchu, Taiwan, in 1985 and his MSEE and PhD degrees from National Taiwan University, Taipei, in 1987 and 1991, respectively. From 1987 to 1989, he was a communication officer with the ROC Army Force. In 1992 he joined the faculty of the Department of Electrical Engineering, Tamkang University, where he is now a professor. From 1998 to 1999, he was a visiting scholar at the Massachusetts Institute of Technology, Cambridge, and the University of Illinois at Urbana-Champaign. He is a visiting professor with the University of Wollongong, Australia, in 2006. Moreover, he was a visiting professor with the University of London, United Kingdom, in 2011. His current research interests include microwave imaging, numerical techniques in electromagnetics, indoor wireless communications, and ultrawideband communication systems. He has published more than 100 journal papers on inverse scattering problems, communication systems and optimization algorithms.

Chi-Hsien Sun received M.S.E.E. and Ph.D degrees in electrical engineering from Tamkang University, Taipei, Taiwan, in 2008 and 2012 respectively. He is now with the Department of ElectronicEngineering, NTUST, as a postdoctoral fellow since 2012. His special interests include theoretical and computational electromagnetics, and application of various optimization schemes such as the steady state genetic algorithm (SSGA), particle swarm optimization (PSO), dynamic differential evolution (DDE), self-adaptive dynamic differential evolution (SADDE) and the Taguchi method in electromagnetics.